



Climate change risk to global port operations

C. Izaguirre¹, I. J. Losada¹✉, P. Camus¹, J. L. Vigh² and V. Stenek¹³

The ports sector is critical to global transport and trade. Climate change may compromise port operations, resulting in an increase in operational shutdowns and subsequent economic losses. Here, we present an analysis of historical global risk across the operations of 2,013 ports worldwide and the impacts under a high-end warming scenario, considering atmospheric and marine hazards, industry established operational thresholds, exposure and vulnerability. Increased coastal flooding and over-topping due to sea level rise, as well as the heat stress impacts of higher temperatures, are the main contributors to amplified risk. Ports located in the Pacific Islands, Caribbean Sea and Indian Ocean appear to be at extremely high risk by 2100, whereas those in the African Mediterranean and the Arabian Peninsula (Persian Gulf and Red Sea) are expected to experience very high risk. Estimating risks at the global scale cannot capture site-level details, but these results provide a benchmark for further research and decision-making.

Ports play an important role in the worldwide economy as essential nodes in the global trading network¹. In addition, they represent long-lasting and critical infrastructure that is sensitive to climate change². Their location along coasts, rivers or lakes involves high exposure to a wide variety of hazards that include sea level rise, changes in extreme sea levels (such as wave set-up or storm surge) and flooding; these hazards may impact the port itself, the regional economy, the operation of supply chains and coastal populations³. Examples are Superstorm Sandy in 2012, which shut down the Port of New York and New Jersey for more than eight days⁴, the floods of 2015 that damaged the Port of Chennai in India⁵, and Hurricane Maria in 2017, which caused infrastructure damage and port shutdown⁶.

Climate change will cause impacts that pose challenges to the well-being of humans and nature². The UNFCCC signed the Paris Agreement in 2015 to enhance mitigation of and adaptation to climate change. Efforts led by the United Nations and growing concerns in the port sector, reflected in initiatives such as the World Ports Climate Declaration and the World Ports Climate Initiative³, have led to enhanced climate resilience through adaptation strategies, although these are still at the planning stage for most seaports⁷.

In the adaptation framework, the necessary first step is risk analysis that addresses the issue of 'adapting to what'². Such an assessment will provide information on the resilience of an existing port or a new investment in the upcoming decades, focusing on the major impacts of climate change that contribute to increased risk in terms of economic, social and environmental consequences. However, few studies have addressed this topic. At the multi-port scale, efforts have been focused on exposure indicators⁸, vulnerability indicators⁹ and perceived risks^{7,10–12}. Other studies that estimate regional economic losses at ports focus on the consequences of disruptions that are due to specific impacts such as tropical cyclones^{13–16}, extreme wind events¹⁷, wave agitation¹⁸, overtopping¹⁹ or sea level rise^{20–22}. Studies that consist of a more detailed assessment of impacts and risk in financial terms are applied to specific cases^{23–32}. However, the multi-hazard risk of climate change in terms of its effects on port operations remains uncertain.

To address this research gap, we estimate future multi-hazard risk in global port operations, including changes in waves, storm surges, wind, precipitation, temperature, tropical cyclones and sea

level rise. The potential impacts associated with these climatic drivers are (1) limitations to manoeuvrability, berthing and load/unload operations owing to high winds, (2) limitations to seaport staff in regard to their ability to work outdoors safely owing to high temperatures, (3) limitations to visibility owing to heavy precipitation, (4) limitations to approach manoeuvres owing to significant wave height, (5) overtopping and (6) coastal flooding limitations to terminal operations, and (7) hits from tropical cyclones. By using an operational threshold approach²³, we link climatic drivers and the resulting impacts to obtain representative multi-hazard frequency indicators. The world's coastal port sector is characterized by 2,013 ports that belong to 172 different nations. The United States, with 211 seaports, is most represented, followed by Japan (149), Indonesia (108) and Canada (99). We select ports using the World Port Index (WPI) database³³. Note that, as we are not considering ports located in rivers, certain important examples such as the Port of Shanghai are not included here. Owing to limited information at the global scale, a number of assumptions are made (see Methods and Supplementary Information).

We use the risk-modelling framework adopted by the IPCC² in which risk is a function of hazard, exposure and vulnerability. For this analysis, the exposure and vulnerability features remain unchanged, and we address future risk by introducing changes in the hazard component for the year 2100 under the high-end emissions pathway, Representative Concentration Pathway 8.5 (RCP8.5)³⁴. We use this approach to highlight the contribution of climate change to risk in port operations in the absence of adaptation. In practice, this provides an upper bound to the risk, given that we expect ports to implement adaptation measures throughout this century to remain competitive in the global trade network. Nevertheless, these insights provide a valuable understanding of approximate trends for individual ports that can inform (i) investors about potential financial, environmental and social considerations and related investments in resilience to optimize the internal rate of return and environmental and social performance, (ii) shippers about the potential reliability of ports (for example, following Hurricane Katrina's impacts on ports in the Gulf of Mexico, some customers shifted to alternative ports³⁵) and (iii) port operators and planners regarding port infrastructure and equipment often designed to last 20 to 50 years, which commits them to coping with several decades of changing climate.

¹IHCantabria-Instituto de Hidráulica Ambiental de la Universidad de Cantabria, Santander, Spain. ²National Center for Atmospheric Research (NCAR), Boulder, CO, USA. ³International Finance Corporation (IFC), World Bank Group, Washington DC, WA, USA. ✉e-mail: losada@unican.es

Meanwhile, this information is useful for assessment of risks at the regional scale (for example, Latin America and Caribbean, or south-eastern Asia–Pacific) or in countries with long coastlines and many ports. Ultimately, this will help identify priority areas for further high-resolution analysis to devise adaptation strategies or even plan the location of new ports in a given network³⁶.

The results show that under present conditions, only ports located in areas prone to tropical cyclones are facing high or very high risk (ports in the Caribbean Sea, eastern Asia or Pacific islands), whereas in the future, climate change will increase risk to very high or extremely high for some ports, mainly those in Indonesia, the Pacific and the Arabian Peninsula.

General methodological framework

The methodology that was undertaken considers RCP8.5 at the end of the current century (an overview is presented in Extended Data Fig. 1). The analysis of each component and the subsequent integration into risk is carried out using a cluster analysis together with a score to obtain results in terms of multi-hazards, vulnerability and risk severity. In terms of the hazards, we identify seven climatic drivers that affect port operations. Marine drivers are combined and processed to obtain nearshore waves (using Snell's law), overtopping (using a semi-empirical formulation) and total water level (as a proxy for coastal flooding), whereas atmospheric drivers are taken as they are. Using an operational threshold approach by selecting operational thresholds, obtaining present and future climate projections, and assessing threshold exceedance frequency, we obtain present and future frequency impact indicators. Exposure is represented by a ranked index that is based on port type and shelter afforded. Vulnerability is formulated by considering a set of port-specific features regarding port services; this set comprises a technological capacity indicator and country-level characteristics pertaining to recovery capacity and resilience. Using a clustering technique and a score approach, we characterize the present multi-hazard severity worldwide and future multi-hazard changes from climate model projections, the sum of which is a measure of future multi-hazard severity. A similar analysis that uses the clustering technique is applied to the vulnerability and the risk, differing from them in the scoring step. This approach, already applied similarly in ref. ³⁷, attempts to go further into the use of the well-established risk index method, which is described in refs. ^{38,39} (see Methods and Supplementary Information for details of these calculations).

Multi-hazard impacts on port operations

We show the present multi-hazard conditions in world port operations across seven primary multi-hazard types and an eighth combined-impact type (Fig. 1). As expected, most ports (42.2%) are located in areas with a low frequency intensity of all impact indicators (Fig. 1c). Ports in Southeast Asia, northeastern United States and the Colombian Pacific Coast are impacted primarily by heavy rain (the ports included in cluster 6 represent 21.6% of the total). Ports in the Caribbean and the Gulf of Mexico, as well as some on the east coast of China, eastern India and Madagascar, are most impacted by tropical cyclones of any category along with heavy rainfall (up to 15.1% of the ports). Note that among the ports in areas prone to tropical cyclones, 9.5% were included in another group that is characterized by a higher probability of tropical cyclone impacts and especially major hurricanes, together with important values of heavy rain impact (ports located in the Philippines, Taiwan, southern Japan and Polynesia). Ports on coasts exposed to heavy wave action, such as those in Morocco, Portugal, northern Spain, France and Ireland in the North Atlantic; those of Namibia and Cape Town (South Africa) in the South Atlantic; those of the west coast of Australia; and those of the north Pacific Coast of the United States (up to 6.3% of the total ports studied), are impacted primarily by agitation in the navigation zone and by heavy rain. A

cluster that consists of 3.5% of the ports identifies the Red Sea and Persian Gulf ports as the most exposed to high temperature. The remaining ports are distributed over two groups. One group represents ports impacted primarily by high winds, located in the Bering Gulf and the Roaring Forties (for example, the port in Stanley in the Falkland Islands). The other group represents ports impacted by a combination of different drivers, such as tropical cyclones, coastal flooding, heavy precipitation, or agitation in the navigation zone as a result of rough waves.

The scoring of the clusters based on the representative non-operability days of each group provides us with a map of the present multi-hazard severity across port operations (Fig. 2a). Ports located in major hurricane-prone areas are considered to be affected with very high-impact severity, and ports in the remaining areas prone to tropical cyclones and heavy rain are assigned high severity. Ports in areas prone to high temperature are assigned intermediate multi-hazard severity.

At the end of the century, the occurrences of coastal flooding, overtopping and high-temperature conditions are predicted to worsen operating conditions most (Extended Data Fig. 2). Coastal flooding and overtopping appear to drive the largest increase in operational disruption, owing primarily to mean sea level rise that affects ports located in the Mediterranean and northern Europe. Ports in Saudi Arabia and the United Arab Emirates will experience a particularly high number of disruptions as a consequence of the increase in extreme temperatures, which negatively affects the safety of workers outdoors. By contrast, ports that historically have been faced with rough wave climate conditions will experience a slight easing of agitation severity at the entrance of the port owing to the projected reduction in significant wave height at mid-latitudes^{40,41}. Finally, by 2100 RCP8.5 is expected to generate a new level of extremely high hazard (Fig. 2b), which was identified mainly among ports located along the coasts of the Arabian Peninsula, southern China, the Philippines, Japan and the Bay of Bengal. Ports in the Mediterranean were also identified as experiencing an increase in impact to a very high level owing to an increase in overtopping conditions.

Present and future risk

The combination of the three components of risk provides a map of the present climate risk for the world port sector (Extended Data Fig. 3). In general, the spatial pattern of risk matches the spatial distribution of the multi-hazard conditions, with several exceptions. Most of the ports present low risk; those at very high risk are located mainly in the Caribbean and Pacific Islands, which are tropical cyclone-prone areas characterized by high exposure and vulnerability. Although the ports with very high multi-hazard severity to port operations in the present day are mostly located in the Philippines, Taiwan and Japan (Fig. 1), these ports do not present very high risk, as their exposure and vulnerability attributes indicate their adaptation to the present climate conditions, especially those in Japan and Taiwan. Up to 44 ports across 21 nations exhibit very high risk historically, with Puerto Rico (8 ports) the most frequently represented (Table 1). Indonesia, the Philippines and Cuba exhibit high risk historically, whereas the United States and Japan exhibit medium risk (Table 1). Among the 854 ports considered to be at medium risk, 50 are classified as large ports in the 2017 WPI, including some crucial nodes in the world trade network such as the ports of Hong Kong, Tokyo, Los Angeles and Rio de Janeiro.

By 2100, RCP8.5 is predicted to change risk for ports around the world. The future distribution of global climate risk for port operations includes increases and decreases in risk level (Fig. 3, varying marker sizes). Changes in mean sea level rise, which create increased overtopping and coastal flooding risk, introduce a new extremely high risk category that contains six ports located in the Pacific, Caribbean Sea and the Indian Ocean (Table 1). At

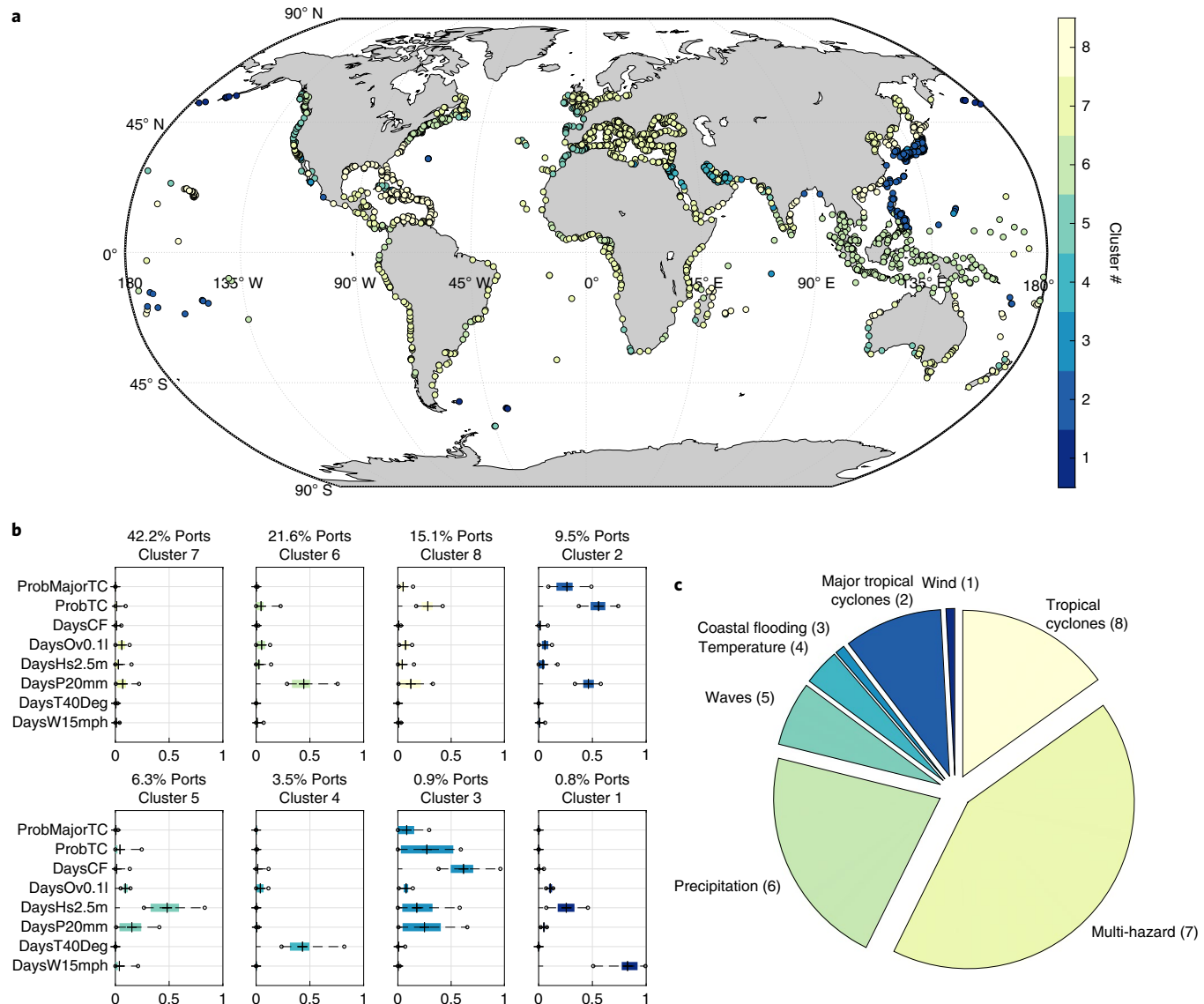


Fig. 1 | Present multi-hazard conditions in world port operations. **a**, Cluster spatial distribution. **b**, Characteristics of the clusters. Each panel contains the percentage of ports included in the cluster, the number of the cluster, the representation of the centroid (cross), the 5th and 95th percentiles of the data of the cluster (points) and the 25th and 75th percentiles of the data of the cluster (coloured bar) on a normalized (0–1) scale for each frequency indicator. ProbMajorTC (in which TC means tropical cyclone), annual exceedance probability of experiencing an SSHWS Category 3 or higher (major hurricane); ProbTC, annual exceedance probability of experiencing an SSHWS Category 1 or higher; DaysCF, average number of days per year with coastal flooding; DaysOv0.1l, number of days per year with overtopping flow $>0.1\text{ m s}^{-1}$; DaysHs2.5m, average number of days per year with significant wave height ($>2.5\text{ m}$) in the navigation zone; DaysP20mm, average number of days per year with heavy precipitation ($>20\text{ mm}$); DaysT40Deg, average number of days per year with daily maximum temperature $\geq 40^\circ\text{C}$; DaysW15mph, average number of days per year with daily mean wind speed $\geq 15\text{ m s}^{-1}$. **c**, Cluster distribution by hazard.

the end of the century, the main change in risk rank occurs in the very high risk category, which increases from 3.8% to 14.4% of the ports. Also striking is the increase in risk for Mediterranean ports, which changes from medium or low risk to very high or high future risk, respectively. Very high risk occurs among the western African Mediterranean ports owing mainly to an increase in overtopping. Increased incidences of high temperature lead to a very high risk rating for ports in the Arabian Peninsula (the Persian Gulf and Red Sea) in the future. To better illustrate the distribution of the ports with increased risk, we provide a detailed view of the Asia-Pacific and Caribbean–North American areas (Figs. 3b,c). The number of ports ranked at very high risk in the future is 283, and they occur mainly in Indonesia, the Philippines, the United States and Japan.

Discussion and conclusions

Using global coverage, our multi-hazard approach offers an initial picture of how climate change risk may evolve under RCP8.5 in the world port network and provides insight into how global maritime trade may be affected. In addition, this information is valuable for international entities such as multilateral agencies and development banks, at both the global and regional scale. This exercise is a first step in assessing risks³⁶ and evaluating the economic consequences of climate change for the port system, and the methodology is adaptable. In addition, risk can be traced backwards at each of the ports analysed, which permits identification of the main drivers that affect operations and the selection of suitable adaptation measures.

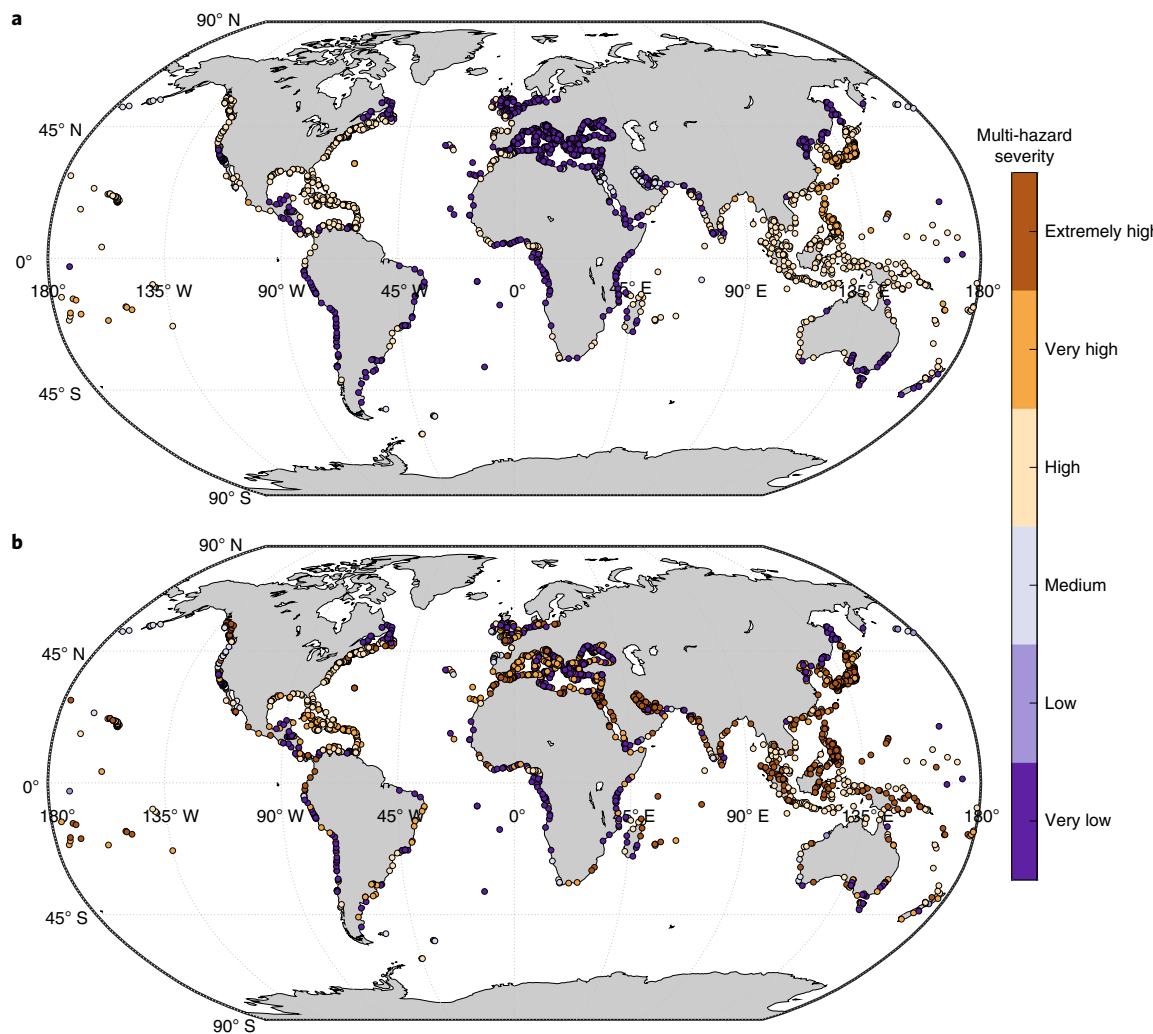


Fig. 2 | Multi-hazard severity across world port operations. a, Present. b, Future (2100, under RCP8.5).

Table 1 | Distribution by country of climate risk levels of port operations

Country position	Extremely high risk		Very high risk		High risk		Medium risk	
	2100 RCP8.5	Historical	2100 RCP8.5	Historical	2100 RCP8.5	Historical	2100 RCP8.5	Historical
1	Aruba (1)	-	Indonesia (25)	Puerto Rico (8)	Indonesia (47)	Indonesia (49)	United States (127)	United States (163)
2	Indonesia (1)	-	Philippines (24)	Bonaire, San Eustaquio y Saba (4)	Philippines (27)	Philippines (28)	Japan (75)	Japan (113)
3	Madagascar (1)	-	United States (21)	Virgin Islands (4)	Japan (25)	Cuba (12)	Italy (53)	Indonesia (59)
4	Palau (1)	-	Japan (18)	Curacao (3)	Nigeria (12)	Nigeria (12)	Canada (42)	Canada (52)
5	Vanuatu (1)	-	Egypt (15)	Marshall Islands (3)	Cuba (11)	Egypt (10)	Indonesia (35)	Philippines (39)
Total global number of ports	6	-	283	44	402	341	883	854

Top five countries at varying degrees of risk, ranked by country position with decreasing number of ports and severity risk. The number of ports that qualify in each category are included in parentheses. Note that the ports projected to experience extremely high risk have no historical precedent, for the highest-risk countries listed.

Previous global studies have considered only proxies such as gross domestic product (GDP) or the population of coastal cities near ports⁸, whereas studies at the regional scale^{9,15} have used simi-

lar indicators from the WPI. Here, we apply cluster analysis to study risk components and the risk itself by grouping indicators. Clusters represent different groupings of conditions and processes that

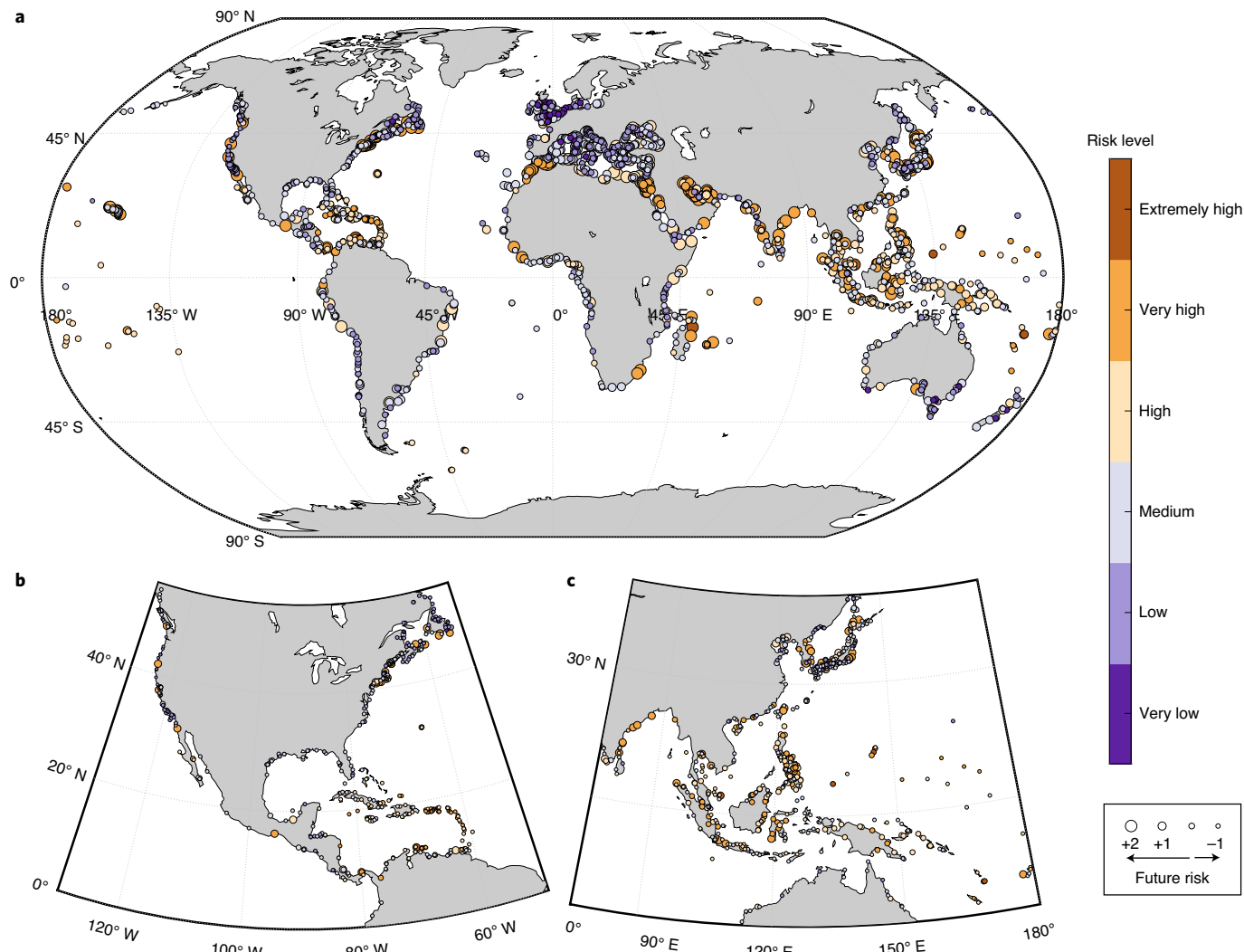


Fig. 3 | Climate risk for the world port sector in the year 2100 under RCP8.5. **a–c,** Details of future climate risk for ports worldwide (**a**), for Caribbean and North American ports (**b**) and for Asia-Pacific ports (**c**). The marker size reflects the change in risk level.

create impacts, vulnerability and risk in the global ports system, which leads to a more comprehensive picture of the factors involved. The advantage of this method, as opposed to a single composite indicator or index, is that it provides richer information on the processes that create and maintain risk components. For example, in the case of multi-hazard conditions, identifying different combinations of frequency impact indicators that cause similar non-operability conditions allows us to detect the main climate drivers that cause disruptions as well as their spatial distribution.

Future assessments should bear in mind the limitations of this study. The multi-hazard approach considers the major climatic drivers (Supplementary Table 1), although this is not comprehensive as other local hazards such as fog or ice are not included. This also applies to the impacts considered, as future changes in water levels and wave patterns may lead to additional impacts on port agitation^{18,29,31,32}, loading and unloading operations, sediment transport patterns and the associated siltation or scouring problems^{23,42,43}, or breakwater stability^{20,44–47}. These impacts are site-specific and require a level of granularity in modelling that cannot be addressed at the global scale. Another limitation arises from the spatial and temporal scale of the global databases of hazard projections. The daily resolution of atmospheric variables in global climate models is limiting when a threshold approach is used to establish

frequency indicators. This was especially true for temperature and was amended by applying expert criteria when possible. However, overestimated agitation, coastal flooding and overtopping for some locations were presumed to occur owing to high waves in the port area. Although wave propagation was carried out to transfer wave climate from deep water to the ports, results are not as expected for all of the ports. We used Snell's law as a propagation method at the global scale. More advanced wave propagation modelling that requires large computational resources and local bathymetric information, together with a detailed description of port infrastructures, would provide more accurate results for wave agitation, overtopping and flooding. However, collecting the required local port information and downscaling waves to local resolution are not feasible at the global scale. Consequently, estimates of wave agitation, overtopping and flooding presented here should be taken as proxies that provide harmonized and comparable results worldwide.

The exposure and vulnerability level have been defined based on the availability of port data at the global scale. Three WPI features were linked to the exposure component by using the channel depth in the propagation of the wave climate from deep water to each port of study and the type of port and shelter afforded. In our approach we assume ports labelled 'coastal breakwater' in the WPI could be considered as protected by rubble-mound breakwaters.

For overtopping results, variations may arise if they are vertical or composite breakwaters instead. The level of vulnerability was addressed by complementing properties related to the technological capacity of each port with indicators related to their recovery capacity and the resilience of the country (GDP per capita and the Logistics Performance Index (LPI)). Note that up to 11 WPI features that represent port services were combined into a technological capacity index, which provides a direct port attribute. Although indices at a national scale do not provide the necessary granularity to resolve the port-scale resolution and may be misleading in some contexts (especially in the developing world), they provide insight into the wealth of the associated country and the perception of the country's logistics performance, which improves the characterization of the vulnerability level. Therefore, the most vulnerable ports are small island state ports, including those of the Lesser Antilles and some on the east coast of Africa, whereas the least vulnerable ports are located in Europe, Japan, and Australia and on the United States Gulf Coast (Extended Data Fig. 4). The WPI database is the most authoritative of its kind in the sector and has been used in other applications^{9,16}. However, some limitations may arise from the scarcity and low accuracy of information in some ports (especially small or very small ports), which can introduce some bias in the vulnerability analysis. To address some of the uncertainties described above, we have made use of expert elicitation (see Supplementary Information).

These results differ from those of previous studies. Among the 2,013 ports considered, we selected (if available) those associated with the 136 largest Organisation for Economic Co-operation and Development (OECD) coastal cities used in ref.⁸ and later in ref.⁴⁸ to assess the port cities with the highest exposure and flood losses. Owing to the different filters that were applied to select our port data sample from the 136 port cities, only 112 were ultimately used in the analysis (see Extended Data Fig. 5 for those at risk in 2100 under RCP8.5). Note that direct comparison is not possible because ref.⁸ considered exposure of port cities to coastal flooding using population and asset indicators as proxies, whereas we address risk by considering multi-hazard impacts and port-specific characteristics to define exposure and vulnerability. The historical risk for some cities in ref.⁴⁸ matches that considered in our study, such as the risk associated with Guayaquil, Abidjan, Zhanjiang and Ho Chi Minh City. Although the comparison of future results is a more difficult task because only changes in flooding were considered, Santo Domingo, Port au Prince, Istanbul, Jakarta and Sapporo were also some of the port cities we found to be at high to very high risk at the end of the century (see Supplementary Table 10 for the present and future risks for the 112 ports linked to the OECD port cities). Ports in coastal cities with major risk level increases include Pusan, Jakarta, Chennai and Durban, all of which shift from medium to very high risk. In addition to those, Kobe, Kawasaki and Yokohama in Japan and Casablanca in Morocco are large ports that experience a risk increase from medium to very high.

Online content

Any methods, additional references, Nature Research reporting summaries, source data, extended data, supplementary information, acknowledgements, peer review information; details of author contributions and competing interests; and statements of data and code availability are available at <https://doi.org/10.1038/s41558-020-00937-z>.

Received: 30 September 2019; Accepted: 22 September 2020;

Published online: 9 November 2020

References

- International Marine Organization (IMO). *International Shipping Facts and Figures – Information Resources on Trade, Safety, Security, Environment* (IMO Maritime Knowledge Center, 2012).
- IPCC: Summary for Policymakers. In *Climate Change 2014: Impacts, Adaptation and Vulnerability* (eds Field, C. B. et al.) (Cambridge Univ. Press, 2014).
- Ng, A. K. Y. et al. Port decision maker perceptions on the effectiveness of climate adaptation actions. *Coast. Manag.* **46**, 148–175 (2018).
- Smythe, T. C. *Assessing the Impacts of Hurricane Sandy on the Port of New York and New Jersey's Maritime Responders and Response Infrastructure*. Quick Response Report No. 238: Final Report to the University of Colorado Natural Hazards Center (2013).
- Becker, A., Ng, A. K. Y., McEvoy, D. & Mullet, J. Implications of climate change for shipping: ports and supply chains. *Wiley Interdiscip. Rev. Clim. Change* **9**, e508 (2018).
- Caribbean Development and Cooperation Committee. *Irma and Maria by Numbers. Focus: ECLAC in the Caribbean* (Economic Commission for Latin America and the Caribbean (ECLAC), 2018).
- Becker, A., Inoue, S., Fischer, M. & Schwegler, B. Climate Change impacts on international seaports: knowledge, perceptions, and planning efforts among port administrators. *Climatic Change* **110**, 5–29 (2012).
- Hanson, S. et al. A global ranking of port cities with high exposure to climate extremes. *Climatic Change* **104**, 89–111 (2011).
- McIntosh, R. D. & Becker, A. Expert evaluation of open-data indicators of seaport vulnerability to climate and extreme weather impacts for U.S. North Atlantic ports. *Ocean Coast. Manag.* **180**, 104911 (2019).
- Mutombo, K. & Ölcer, A. Towards port infrastructure adaptation: a global port climate risk analysis. *WMU J. Marit. Aff.* **16**, 161–173 (2017).
- O'Keeffe, J. M., Cummins, V., Devoy, R. J. N., Lyons, D. & Gault, J. Stakeholder awareness of climate adaptation in the commercial seaport sector: a case study from Ireland. *Mar. Policy* **111**, 102404 (2020).
- Yang, Z. et al. Risk and cost evaluation of port adaptation measures to climate change impacts. *Transportation Res. D* **61B**, 444–458 (2018).
- Esteban, M., Webersik, C. & Shibayama, T. Methodology for the estimation of the increase in time loss due to future increase in tropical cyclone intensity in Japan. *Climatic Change* **102**, 555–578 (2010).
- Esteban, M., Thao, N., Takagi, H. & Shibayama, T. Increase in port downtime and damage in Vietnam due to a potential increase in tropical cyclone intensity. In *Climate Change and the Sustainable Use of Water Resources* (ed. Leal Filho, W.) 101–125 (Springer, 2012).
- Lam, J. S. L., Liu, C. & Gou, X. Cyclone risk mapping for critical coastal infrastructure: cases of East Asian seaports. *Ocean Coast. Manag.* **141**, 43–54 (2017).
- Jian, W., Liu, C. & Lam, J. S. L. Cyclone risk model and assessment for East Asian container ports. *Ocean Coast. Manag.* **178**, 104796 (2019).
- Zhang, Y. & Lam, J. S. L. Estimating the economic losses of port disruption due to extreme wind events. *Ocean Coast. Manag.* **116**, 300–310 (2015).
- Sierra, J. P., Casas-Prat, M., Virgili, M., Mössö, C. & Sánchez-Arcilla, A. Impacts on wave-driven harbour agitation due to climate change in Catalan ports. *Nat. Hazards Earth Syst. Sci.* **15**, 1695–1709 (2015).
- Sierra, J. P., Casanovas, I., Mössö, C., Mestres, M. & Sánchez-Arcilla, A. Vulnerability of Catalan (NW Mediterranean) ports to wave overtopping due to different scenarios of sea level rise. *Reg. Environ. Change* **16**, 1457–1468 (2015).
- Becker, A., Chase, N. T. L., Fischer, M., Schwegler, B. & Mosher, K. A method to estimate climate-critical construction materials applied to seaport protection. *Glob. Environ. Change* **40**, 125–136 (2016).
- Gracia, V. et al. Assessing the impact of sea level rise on port operability using LiDAR-derived digital elevation models. *Remote Sens. Environ.* **232**, 111318 (2019).
- Christodoulou, A., Christidis, P. & Demirel, H. Sea-level rise in ports: a wider focus on impacts. *Marit. Econ. Logist.* **21**, 482–496 (2019).
- Monioudi, I. N. et al. Climate change impacts on critical international transportation assets of Caribbean Small Island Developing States (SIDS): the case of Jamaica and Saint Lucia. *Reg. Environ. Change* **18**, 2211–2225 (2018).
- Stenek, V. et al. *Climate Risk and Business Ports: Terminal Marítimo Muelles el Bosque, Cartagena, Colombia* (International Finance Corporation, 2011).
- Chhetri, P., Jayatilleke, G., Gekara, V., Manzoni, A. & Corbitt, B. J. Container terminal operations simulator (CTOS) – simulating the impact of extreme weather events on port operation. *Eur. J. Transp. Infrastruct. Res.* **16**, 195–213 (2016).
- Morris, L. L. & Sempier, T. *Ports Resilience Index: A Port Management Self-Assessment* (U.S. Department of Commerce, 2016).
- Zhang, H. & Ng, A. The regional efforts of Port Metro Vancouver in adapting to potential impacts posed by climate change. In *Proc. Annual Conference of the International Association of Maritime Economists (IAME)* (2016).
- Connell, R. et al. *Port of Manzanillo: Climate Risk Management* (Inter-American Development Bank, 2015).
- Campos, Á. et al. Addressing long-term operational risk management in port docks under climate change scenarios – a Spanish case study. *Water* **11**, 2153 (2019).

30. Messner, S., Moran, L., Reub, G. & Campbell, J. Climate change and sea level rise impacts at ports and a consistent methodology to evaluate vulnerability and risk. *WIT Trans. Ecol. Environ.* **169**, 141–153 (2013).
31. Sierra, J. P. et al. Modelling the impact of climate change on harbour operability: the Barcelona port case study. *Ocean Eng.* **141**, 64–78 (2017).
32. Camus, P. et al. Probabilistic assessment of port operation downtimes under climate change. *Coast. Eng.* **147**, 12–24 (2019).
33. *World Port Index* (National Geospatial-Intelligence Agency, 2017).
34. Riahi, K. et al. RCP 8.5—a scenario of comparatively high greenhouse gas emissions. *Climatic Change* **109**, 33–57 (2011).
35. Grenzeback, L. R. & Lukmann, A. T. *Case Study of the Transportation Sector's Response to and Recovery from Hurricanes Katrina and Rita* (Cambridge Systematics, 2008).
36. Izaguirre, C., Losada, I. J., Camus, P., González-Lamuño, P. & Stenek, V. Seaport climate change impact assessment using a multi-level methodology. *Marit. Policy Manag.* **47**, 544–557 (2020).
37. Calil, J., Reguero, B. G., Zamora, A. R., Losada, I. J. & Méndez, F. J. Comparative Coastal Risk Index (CCRI): a multidisciplinary risk index for Latin America and the Caribbean. *PLoS ONE* **12**, e0187011 (2017).
38. Alexandrakis, G. & Poulos, S. E. An holistic approach to beach erosion vulnerability assessment. *Sci. Rep.* **4**, 6078 (2014).
39. Balica, S. F., Wright, N. G. & van der Meulen, F. A flood vulnerability index for coastal cities and its use assessing climate change impacts. *Nat. Hazards* **64**, 73–105 (2012).
40. Camus, P. et al. Statistical wave climate projections for coastal impact assessments. *Earth's Future* **5**, 918–933 (2017).
41. Morim, J. et al. Robustness and uncertainties in global multivariate wind-wave climate projections. *Nat. Clim. Change* **9**, 711–718 (2019).
42. Sánchez-Arcilla, A. et al. A review of potential physical impacts on harbours in the Mediterranean Sea under climate change. *Reg. Environ. Change* **16**, 2471–2484 (2016).
43. Sierra, J. P. & Casas-Prat, M. Analysis of potential impacts on coastal areas due to changes in wave conditions. *Climatic Change* **124**, 861–876 (2014).
44. Mase, H., Tsujio, D., Yasuda, T. & Mori, N. Stability analysis of composite breakwater with wave-dissipating blocks considering increase in sea levels, surges and waves due to climate change. *Ocean Eng.* **71**, 58–65 (2013).
45. Suh, K.-D., Kim, S.-W., Mori, N. & Mase, H. Effect of climate change on performance-based design of caisson breakwaters. *J. Waterw. Port. Coast. Ocean Eng.* **138**, 215–225 (2012).
46. Esteban, M., Takagi, H. & Shibayama, T. Sea level rise and the increase in rubble mound breakwater damage. In *Proc. 6th International Conference on Coastal Structures* 130–140 (World Scientific, 2013).
47. Takagi, H., Kashihara, H., Esteban, M. & Shibayama, T. Assessment of future stability of breakwaters under climate change. *Coast. Eng. J.* **53**, 21–39 (2011).
48. Hallegate, S., Green, C., Nicholls, R. J. & Corfee-Morlot, J. Future flood losses in major coastal cities. *Nat. Clim. Change* **3**, 802–806 (2013).

Publisher's note Springer Nature remains neutral with regard to jurisdictional claims in published maps and institutional affiliations.

© The Author(s), under exclusive licence to Springer Nature Limited 2020

Methods

World coastal port sector. We used the 26th edition of Pub 150 (the WPI)³³, developed by the National Geospatial-Intelligence Agency. This data set provides the location, characteristics, known facilities and available services of ports, shipping facilities and oil terminals throughout the world (approximately 3,700 entries). From the full data set, we considered only open coast ports, including the coastal natural, coastal breakwater, coastal tide gate, open roadstead and typhoon types. We excluded environments dominated by rivers and estuaries, thereby eliminating all of the ports located in rivers, lakes or canals. In addition, we filtered out all of the ports that have no information on harbour type, size or shelter afforded, as well as harbours and stations located in Antarctica (as they are not considered part of the global trade network) and some very small ports located in Tierra del Fuego. This led to a final set of 2,013 seaports worldwide.

After analysing all of the available attributes for each of the 2,013 ports, we selected the following for exposure characterization: longitude and latitude of the port location, type of harbour and channel depth. Coordinates and channel depth information, which refer to the controlling depth of the principal or deepest channel, were used when propagating the wave climate. The harbour type and shelter afforded were used to obtain the level of exposure to multi-hazards (see Supplementary Information, Supplementary Table 6 and Extended Data Fig. 6). For the vulnerability analysis, we extracted the country code and information on the port size, estimated time of arrival message, pilotage, tugs, communications, medical facilities, garbage disposal, cranes or lifts, services, supplies, repairs, and dry docks or marine railways. The information on all of these port service features was combined into an indicator pertaining to the technological capacity of the port (Supplementary Table 7).

Frequency impact indicators. Wind, temperature, precipitation, waves, storm surge, sea level rise and astronomical tide, or a combination of these variables (for example, to describe wave overtopping) have been identified to produce operational disruptions when exceeding given thresholds. Following ref. ²³, generic thresholds (suitable for assessment at the global scale) were selected based on national or international recommendations. Impact frequency indicators were defined and deemed to be representative of impacts (see Supplementary Table 1 and below for a detailed description). In the case of tropical cyclones, we decided to use two frequency indicators to assess the hazards for areas exposed to cyclones: the annual exceedance probability of experiencing wind gusts that exceed 118 kt (60.7 m s^{-1}) at the location of the port from a tropical cyclone of Saffir–Simpson Hurricane Wind Scale (SSHWS) Category 1 or higher, and the annual exceedance probability of experiencing wind gusts that exceed 118 kt corresponding approximately, in this case, to a tropical cyclone of an SSHWS Category 3 or higher (see Supplementary Information section ‘Estimation of TC climate indicators’ for more information). All of the indicators were developed within the framework of the ‘Climate Risk Management: Ports and Water Transport’ project funded by the International Finance Corporation (IFC) of the World Bank Group.

The included oceanic drivers of impact were waves for port agitation and the combination of waves, storm surge, astronomical tide, mean sea level anomalies and sea level rise for overtopping and coastal flooding. We obtained overtopping values from ref. ⁴⁹, whereas for coastal flooding we used the total water level to represent the maximum potential flood hazard in a berth with a freeboard of 0.6 m at present. Historical information for waves was obtained from the GOW2 database³⁴ and was propagated to the channel depth. Data on historical storm surges were obtained from the global database Dynamic Atmospheric Correction by Aviso, astronomical tide information was obtained by using harmonic analysis from the outcomes of the global model of ocean tides (TPXO8⁵¹), and historical mean sea level data were obtained by using the method proposed in ref. ⁵².

The RCP8.5 projection data for regional mean sea level were obtained from ref. ⁵³ and result from changing ocean circulation, increased heat uptake and atmospheric pressure in climate models of the Coupled Model Intercomparison Project Phase 5 (CMIP5). However, local land subsidence was not included (see Supplementary Information for more details). Projections of frequency impact indicators under RCP8.5 for the end of the century came from a multi-model ensemble of CMIP5 (ref. ⁵⁴) by using the mean of the probability distribution of the projected drivers or indicators, therefore considering several runs and global climate models and thereby limiting uncertainty. Projections from marine variables were calculated at the Instituto de Hidráulica Ambiental Cantabria (IHCantabria) following ref. ⁴⁰ by using statistical downscaling based on the weather typing approach, whereas projections from atmospheric variables were computed at the National Center for Atmospheric Research (NCAR) (see Supplementary Information for a more detailed description). Limitations of the daily temporal resolution of global climate models arise here, as thresholds may apply to a lower temporal scale; for example, an employee’s ability to work safely outdoors is limited when the temperature exceeds 40 °C, but this exceedance will probably occur only during certain hours and not during the whole day.

Tropical cyclones are also a main driver of operational disruptions or even the reason for the closure of a port owing to extreme conditions associated with waves, storm surge, winds and precipitation. The frequency indicator related to tropical cyclones is based on the annual exceedance probability of experiencing different

categories of tropical cyclones. The analysis of historical wind and pressure fields was carried out at the NCAR using the Australia Geoscience Tropical Cyclone Risk Model (TCRM), which is a stochastic tropical cyclone model developed for estimating wind hazards from tropical cyclones (see Supplementary Information for more detail). Projections of future tropical cyclones were obtained by applying results from the literature and adding 1.0% per decade to the maximum sustained winds, which is roughly the level of intensity increases that could be expected under the RCP8.5 scenario⁵⁵.

Multi-hazard patterns. The *k*-means clustering technique⁵⁶ was used to process the large amount of spatial information regarding frequency impact indicators that are related to the operation of the port sector (see Supplementary Information for a more detailed description). Therefore, the application to a sample of 16,104 data points (2,013 ports \times 8 historical impact indicators) provided different clusters, including specific impact conditions, that revealed the existence of clear patterns around the world. Owing to sea level rise, the overtopping frequency indicator will be increased in the future, but at present it is assumed not to be a risk contributor because coastal breakwaters were designed not to be overtopped under historical conditions.

Different sensitivity tests were carried out to obtain the best results in terms of the definition of groups using eight clusters (Fig. 1). To validate these results, a review of historical disruption events was conducted, which corroborated evidence of the main drivers of stoppage in different parts of the world (Extended Data Fig. 7 and Supplementary Table 3). The next step involved assigning scores to each cluster based on the days of stoppage of the maximum hazard of the centroid (Supplementary Table 4) and making several assumptions. Cluster 4, whose maximum impact value of the centroid corresponds to days of stoppage due to a daily maximum temperature $\geq 40^\circ\text{C}$, is associated with 42 days per year of stoppage. To consider more realistic data, we divided the centroid value by 2.5, considering that the maximum daily temperature occurs during less than half of the day. Cluster 5, in which the maximum impact value centroid refers to the days of stoppage due to a significant wave height $> 2.5 \text{ m}$ in the navigation zone, presents stoppage of 69 days per year. Foreseeably, this high value is due to very high waves in the port owing to the propagation approach. Although we propagated wave height from deep water into shallow water, Snell’s law as applied here shows a very low reduction in wave height. Instead of using this misleading value of the centroid, we considered 20 days per year to be appropriate, which is the maximum closure period accepted by the Spanish Recommendations for Maritime Works ROM3.1-99 in port design. For clusters 2 and 8, in which the maximum hazard of the centroid is tropical cyclone probability, the days of stoppage were obtained by assuming a simple relationship with the frequency of tropical cyclones. We considered that every port closes one day before the cyclone hits, and remains closed during its passage (which is considered to last one day) and for 20 days afterwards. The review of historical events and stoppages shows wide variation in the number of days of disruption depending on the port and the hurricane category, with an average time of 15 days of port closure. Taking into account this information and the goal of estimating an indicative number of days based on the probability of experiencing a hurricane of Category 1 or higher, we make the assumption of an average time of disruption after the passage of the cyclone of 20 days (Category 1 or higher). The assignment of the minimum score (of 1) to three days of stoppage (cluster 7) and the maximum score (of 5) to 23 days of stoppage (cluster 2) leads to a 20-day range. When this range is divided into four equal steps, every five days of increase or decrease of stoppage correspond to a unit of change in score. Applying this relationship, we score the groups (Supplementary Table 4). Although cluster 8 has 12 days of stoppage, which is fewer than for the other clusters, we give this cluster a high score (of 4) owing to the extreme and usually catastrophic nature of the event.

Future changes in frequency impact indicators were analysed following a similar approach that combined *k*-means clustering and a ranking scale. Future changes in impact were first transformed by using the expression $i' = \frac{i_f - i_p}{i_{p\max} - i_{f\max}}$, where i' is the normalized change in impact, i_p is the value of the impact in the future (2100), i_f is the present value of the impact, $i_{p\max}$ is the current maximum spatial impact value and $i_{f\max}$ is the maximum spatial impact value in the future. They were also normalized next by using $i'' = \frac{i'}{\max(|\max(i')|, |\min(i')|)}$ with values ranging from -0.5 to 0.5 and by taking into account the positive or negative relative change. Using the results of the first transformation, we considered the relative change in the impacts by weighting the magnitude of their future value, giving more importance to changes that result in higher impact values. After testing different numbers of clusters, nine comprised the groups that best represent changes in impact conditions (Extended Data Fig. 8). Finally, we scored the groups by taking into account the maximum change in the maximum hazard defining the centroid (for example, in cluster 1, the maximum change corresponds to the wind impact) that is transformed into an increase or decrease in the number of days of stoppage, worsening or improving the impact conditions. The score followed the same criteria as in Supplementary Table 4. In group 9, the maximum impact that defines the centroid corresponds to the overtopping driver (expressed in Supplementary Table 5 as 9(5), leading to an increase in stoppage of 22.3 days per year). We considered this driver only for ports with breakwater infrastructure, which account for 21.8% of the ports. Ports included in cluster 9 but without

breakwater are represented by the next maximum frequency impact indicator value of the centroid, which in this case corresponds to precipitation (referred to as 9(3)) and leads to an increase of two days per year of stoppage.

The multi-hazard conditions that affect port operations at the end of the century (RCP8.5) were obtained by adding the scored future changes to the historical ranking score. With this approach, the ranking score range from 1 to 5 was broadened to 1 to 8 (with floating-point numbers), which allowed us to introduce a new category of extremely high impact (score >5.5).

Vulnerability level. Three indicators are considered to define vulnerability: technological capacity, recovery capacity and resilience. Technological capacity is measured through the services provided by each port. The indicator is built by adding eleven attributes extracted from the WPI (Supplementary Table 7). For a given attribute, WPI reports 1 (available) or 0 (not available). If no information is provided, we assume that the service is not available. Consequently, a port with high technological capacity (all of the services available) will score 11 for this indicator and 0 if no technological capacity is in place. The GDP per capita is an indicator of country's wealth and may be used as a proxy to provide information regarding the recovery capacity of its assets⁵⁷. The information that we used was obtained from the World Bank national accounts data and OECD National Accounts Statistics data files and is expressed in 2017 US\$. As a proxy for resilience, we used the LPI, which is an indicator that reflects perceptions of a country's logistics performance. The index ranges from 1 to 5, with the highest score representing the best performance. Data were obtained from LPI surveys that are conducted by the World Bank in partnership with academic and international institutions, private companies and individuals engaged in international logistics (<https://datacatalog.worldbank.org/dataset/logistics-performance-index>). We analysed the vulnerability conditions of each port by applying the clustering technique to the three indicators that are considered to define vulnerability. These triplets of variables were clustered into six groups (Extended Data Fig. 9). As an example, cluster 4, which is characterized by moderate to high recovery capacity, high resilience and high technological capacity, represents ports on the east and west coasts of the United States, some ports in Japan and others in Australia. By contrast, cluster 6 represents Pacific Island ports, some Caribbean ports and some ports in Africa that are characterized by a low recovery capacity, very low resilience and intermediate technological capacity. We transformed the six clusters into a 1 to 5 ranked scale (very low to very high vulnerability) by using the sum of the three-value centroids of each cluster as an indicator of the severity of its vulnerability. The maximum sum of the three normalized components was divided into five ranges within which the sum of the three-value centroids was classified, leading to the ranked scale (Supplementary Table 8).

Risk conditions. The integration was performed by using the *k*-means clustering technique applied to the ranked level of exposure, vulnerability and impact under the present conditions. After a sensitivity analysis (see Supplementary Information), we identified the 10 groups that best represent the existing combinations of hazard, exposure and vulnerability and therefore risk conditions around the world (Extended Data Fig. 10). Next, we scored the groups on a scale of 1 to 5, where 1 indicates very low risk and 5 indicates very high risk, to obtain a final ranked risk index (Supplementary Table 9). The scoring is based on the sum of the three components of the centroid. The present risk in the global port sector is provided (Extended Data Fig. 3).

The risk at the end of the century and under RCP8.5 was estimated by projecting future combinations of hazard *H*, exposure *E* and vulnerability *V* onto the 10 historical clusters of risk that were found. With this approach, we could determine whether changes in hazards and their related impacts result in changes in the representative cluster for a given port. Future values of each impact were normalized by using the minimum and maximum values that were used in the historical grouping, whereas the exposure and vulnerability dimensions remained as they were under historical conditions. The ports included in clusters 2, 3, 4 and 8, which are characterized by low historical impact conditions, will be able to shift into groups 5, 10, 7 and 1, respectively, owing to an increase in the impact conditions, as they have similar exposure and vulnerability characteristics but higher future hazard conditions. The new cluster associated with each port was that for which the Euclidean distance between the three-dimensional data and the centroid was minimal. However, the ports historically assigned to clusters 1, 5, 6, 7, 9 and 10, which show high values of historical impact, will not be able to shift into another group if future hazard conditions increase. Consequently, if a change in the score is needed because the Euclidean distance to the centroid of the original cluster is greater than the historical maximum distance, an increase in the score is provided by using $\sum_{0.6}^{(H_E, E, V)_{\text{port}} - \sum_{0.6}^{(H_E, E, V)_{\text{centroid}}}}$, where the triplet of the port refers to future conditions, the triplet of the centroid refers to the centroid of the present risk group, and 0.6 stands for the score step in the risk scoring range. This will lead to a new class of extremely high risk identified for the future, which broadens the 1 to 5 ranked scale of risk to a 1 to 6 scale. However, only ports with very high exposure and vulnerability, or those with very high future hazard and either very high exposure or vulnerability, will reach this risk category.

Expert elicitation. Some of the uncertainties inherent in working at a global scale using indicators, the assumptions made and the lack of data can be reduced beneficially by the added value of expert elicitation. In this work, expert elicitation served two main purposes: the validation of a preliminary selection of indicators for climate and extreme hazards, exposure and vulnerability, and the establishment of correlations between scoring and their corresponding hazard, exposure, vulnerability and risk levels (see Supplementary Information for details on the process and its limitations).

Data availability

The atmospheric and marine frequency impact indicators that support the findings of this study are available from the IFC and were used under licence for the current study. Data are available from the authors upon request by contacting iidata@ihcantabria.es, if permission from the IFC is granted.

Code availability

Computer codes or algorithms used to generate results that are reported in the paper and central to its main claims are available at: <https://doi.org/10.5281/zenodo.3987516>.

References

49. Owen, M. W. *Design of Seawalls Allowing for Wave Overtopping*, Report No. EX924 (Hydraulics Research Wallingford, 1982).
50. Perez, J., Menendez, M. & Losada, I. J. GOW2: a global wave hindcast for coastal applications. *Coast. Eng.* **124**, 1–11 (2017).
51. Egbert, G. D. & Erofeeva, S. Y. Efficient inverse modeling of barotropic ocean tides. *J. Atmos. Ocean. Technol.* **19**, 183–204 (2002).
52. Church, J. A., White, N. J., Coleman, R., Lambeck, K. & Mitrovica, J. X. Estimates of the regional distribution of sea level rise over the 1950–2000 period. *J. Clim.* **17**, 2609–2625 (2004).
53. Slanger, A. B. A. et al. Projecting twenty-first century regional sea-level changes. *Climatic Change* **124**, 317–332 (2014).
54. Taylor, K. E., Stouffer, R. J. & Meehl, G. A. An overview of CMIP5 and the experiment design. *Bull. Am. Meteorol. Soc.* **93**, 485–498 (2012).
55. Villarini, G. & Vecchi, G. A. Projected increases in North Atlantic tropical cyclone intensity from CMIP5 models. *J. Clim.* **26**, 3231–3240 (2013).
56. Camus, P., Méndez, F. J., Medina, R. & Cofiño, A. S. Analysis of clustering and selection algorithms for the study of multivariate wave climate. *Coast. Eng.* **58**, 453–462 (2011).
57. Koks, E. E. et al. A global multi-hazard risk analysis of road and railway infrastructure assets. *Nat. Commun.* **10**, 2677 (2019).

Acknowledgements

We acknowledge the support from the Spanish Ministerio de Economía y Competitividad (MINECO) under the RISKOADAPT project (grant no. BIA2017-89401-R). We are grateful to C. Amman for his work in the development of atmospheric frequency impact indicators and A. Espejo for his useful comments. The atmospheric and marine frequency impact indicators have been developed jointly by NCAR and IH Cantabria with the financial support of the IFC. This material is based in part on work supported by the NCAR, which is a major facility sponsored by the National Science Foundation under cooperative agreement no. 1852977. Computing resources were provided by the Climate Simulation Laboratory at the NCAR Computational and Information Systems Laboratory. We acknowledge the Working Group on Coupled Modelling of the World Climate Research Programme, which is responsible for the CMIP, and we thank the climate modelling groups for producing and making available their model output.

Author contributions

I.J.L. conceived the study and designed it with C.I. and P.C. jointly. C.I. and P.C. performed the analysis and developed the marine frequency indicators. J.L.V. developed the atmospheric frequency indicators. C.I., I.J.L. and V.S. wrote the manuscript. All of the authors contributed to make substantial improvements to the manuscript.

Competing interests

The authors declare no competing interests.

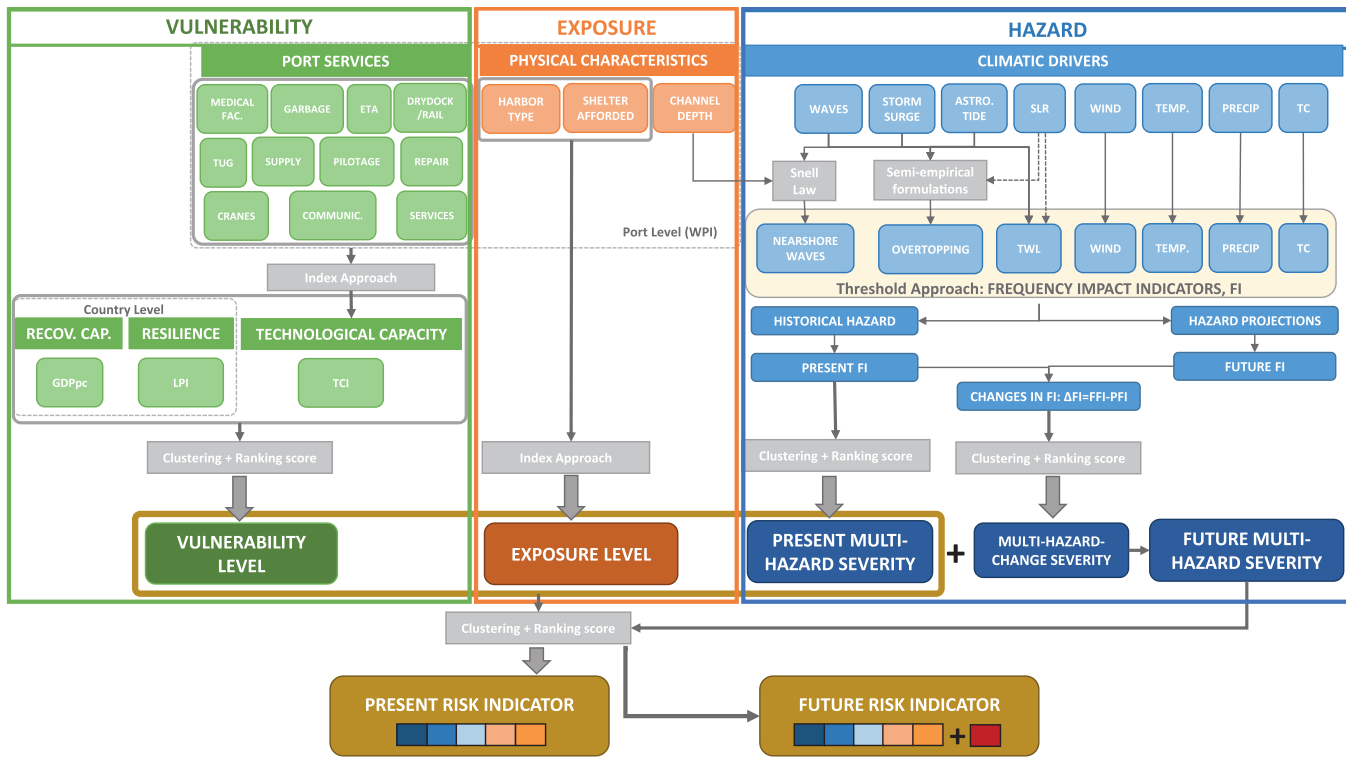
Additional information

Extended data is available for this paper at <https://doi.org/10.1038/s41558-020-00937-z>.

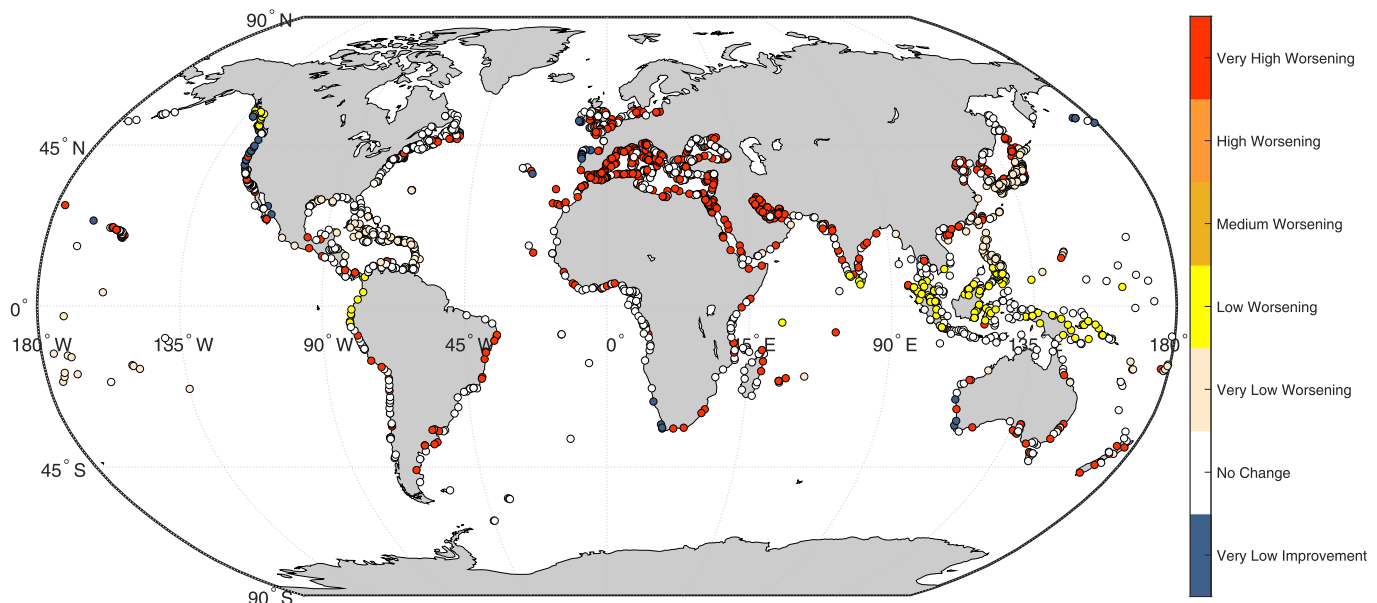
Supplementary information is available for this paper at <https://doi.org/10.1038/s41558-020-00937-z>.

Correspondence and requests for materials should be addressed to I.J.L.

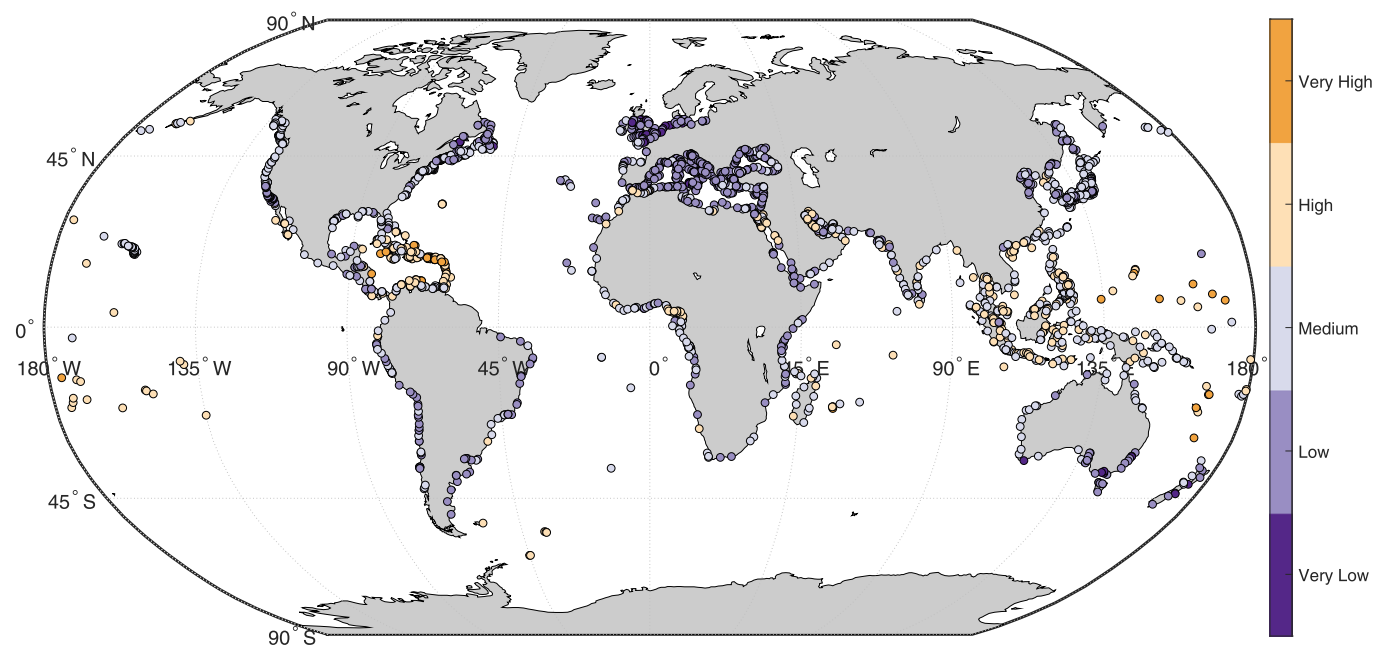
Peer review information *Nature Climate Change* thanks Austin Becker, Robert Nicholls, Joan Pau Sierra and the other, anonymous, reviewer(s) for their contribution to the peer review of this work. **Reprints and permissions information** is available at www.nature.com/reprints.



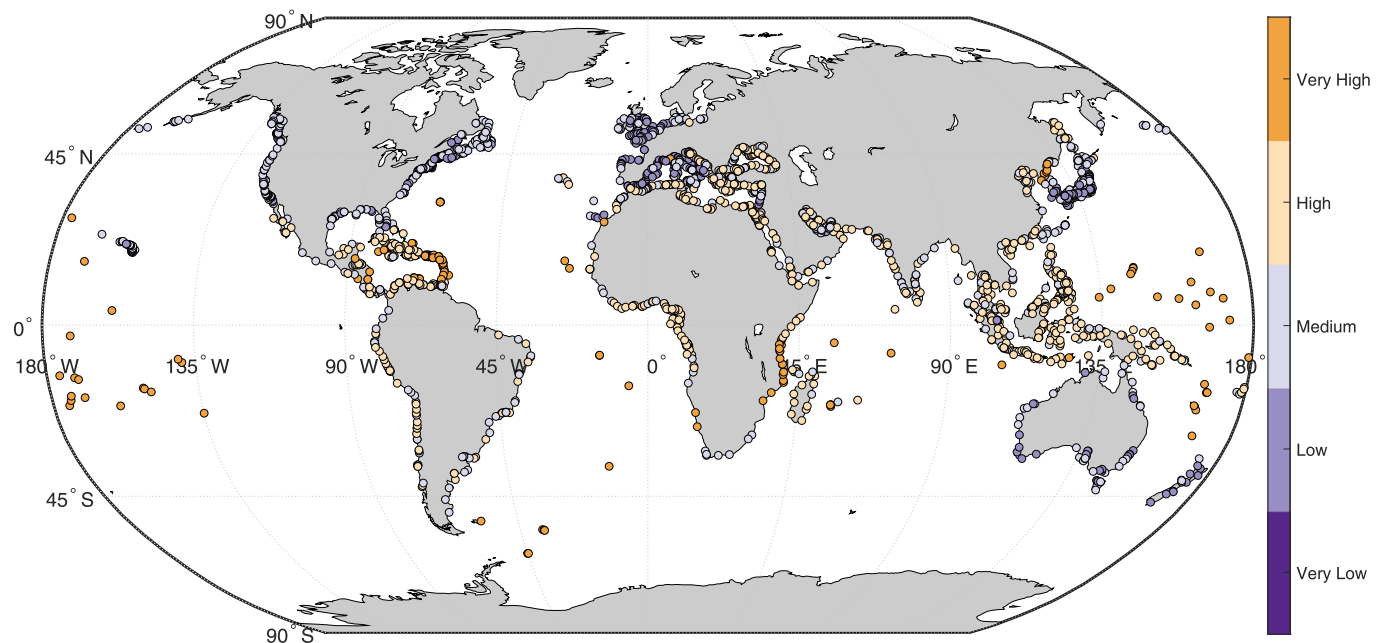
Extended Data Fig. 1 | Methodological overview of study. Green colour represents vulnerability variables/indicators used and produced, orange represents exposure characteristics, and blue represents hazard variables/indicators. Grey boxes and arrows indicate the method/approach used for analysing information.



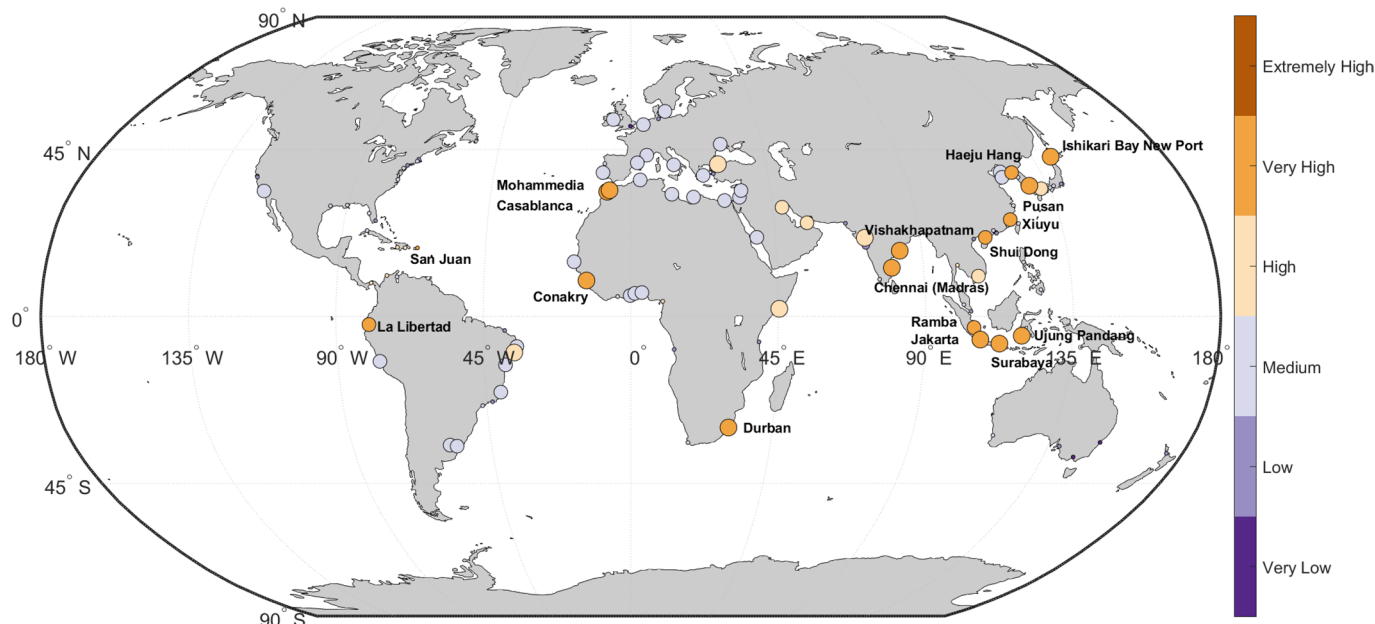
Extended Data Fig. 2 | Future change in multihazard severity. Multihazard change severity for each port in the year 2100 under RCP8.5 in terms of the improvement and worsening of present multihazard conditions.



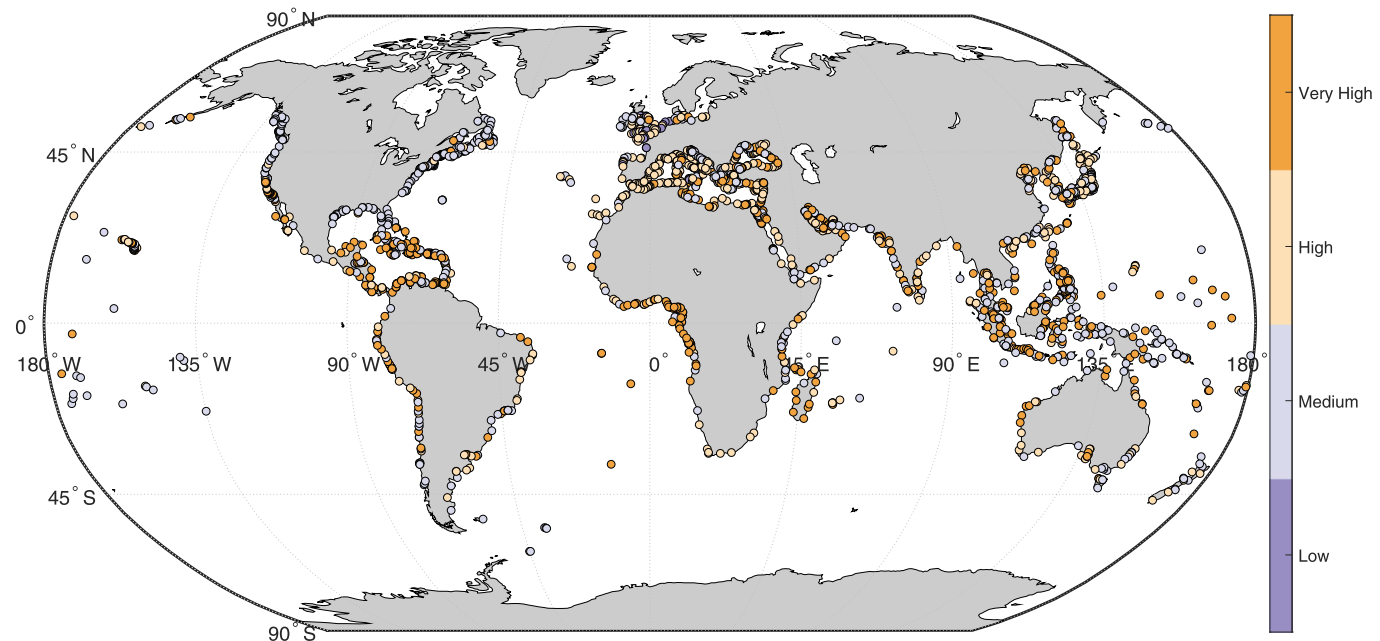
Extended Data Fig. 3 | Present risk level. Present-day risk levels shown for all ports.



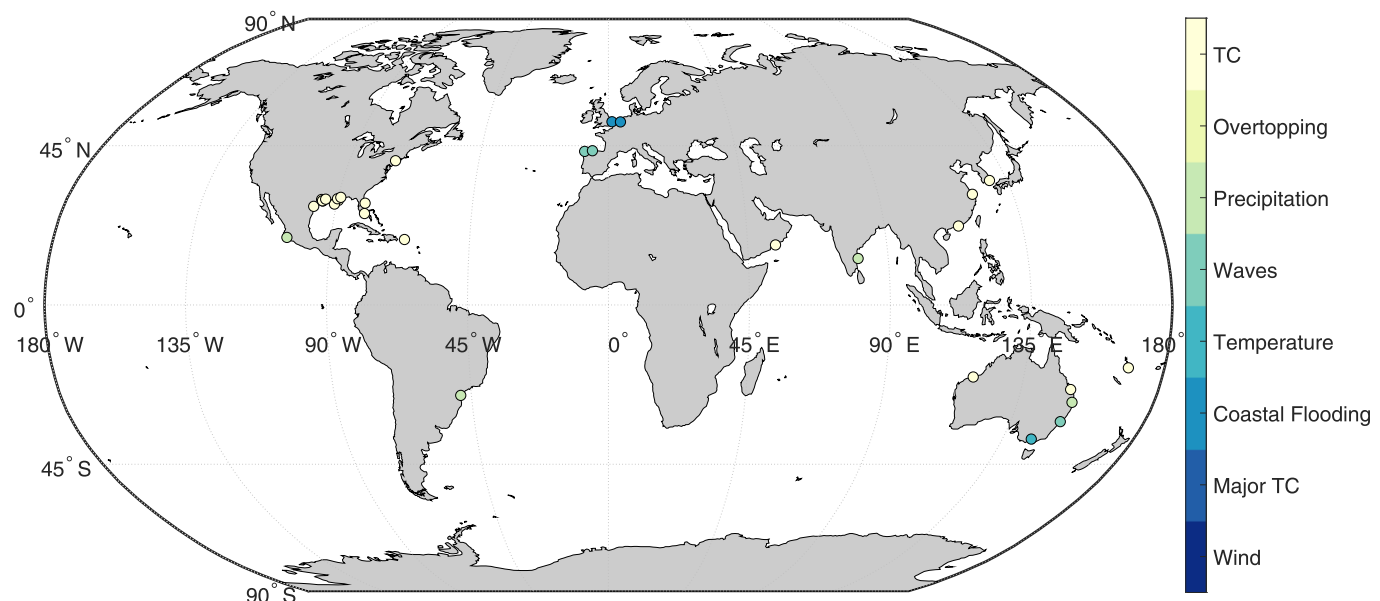
Extended Data Fig. 4 | Present vulnerability level. Present vulnerability level shown for each port.



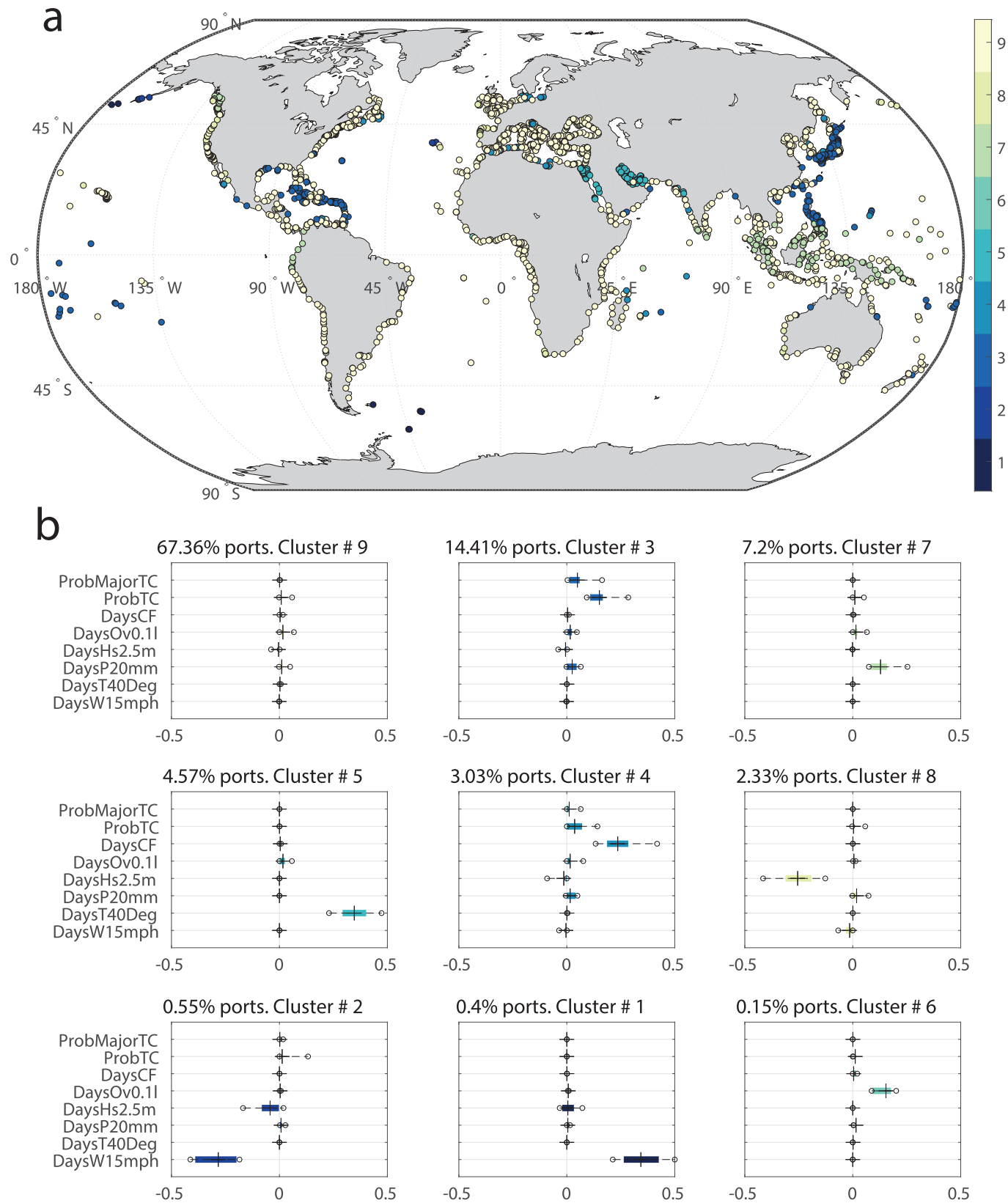
Extended Data Fig. 5 | Future risk levels. Climate risk in the year 2100 under RCP8.5 across the operations of the largest OECD port cities. Marker size indicates the change in risk level.



Extended Data Fig. 6 | Present exposure level. Present-day exposure level shown for each port.

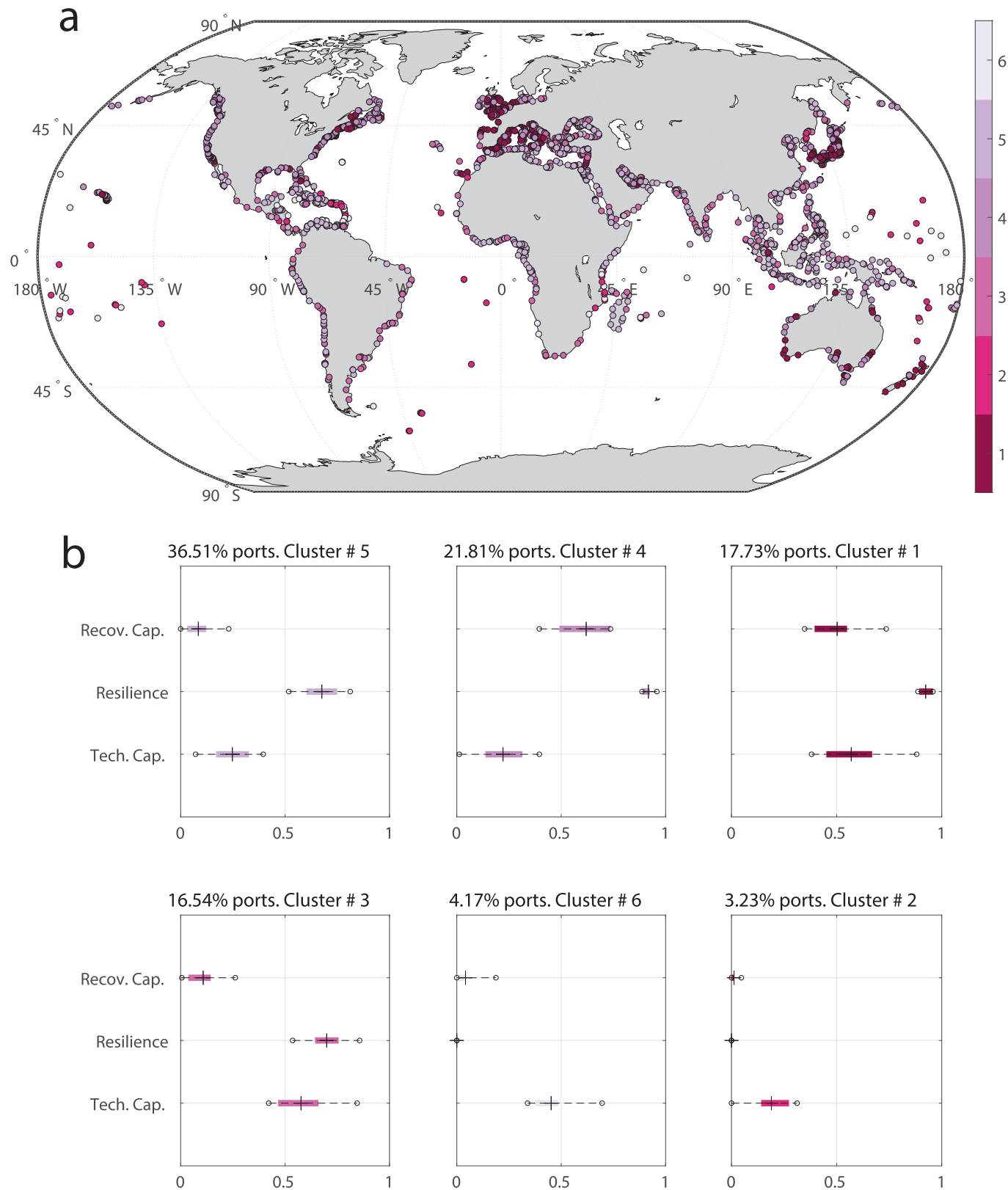


Extended Data Fig. 7 | Dominant climatic drivers of port disruptions. Spatial representation of dominant climatic drivers of port disruptions in 30 locations around the world.

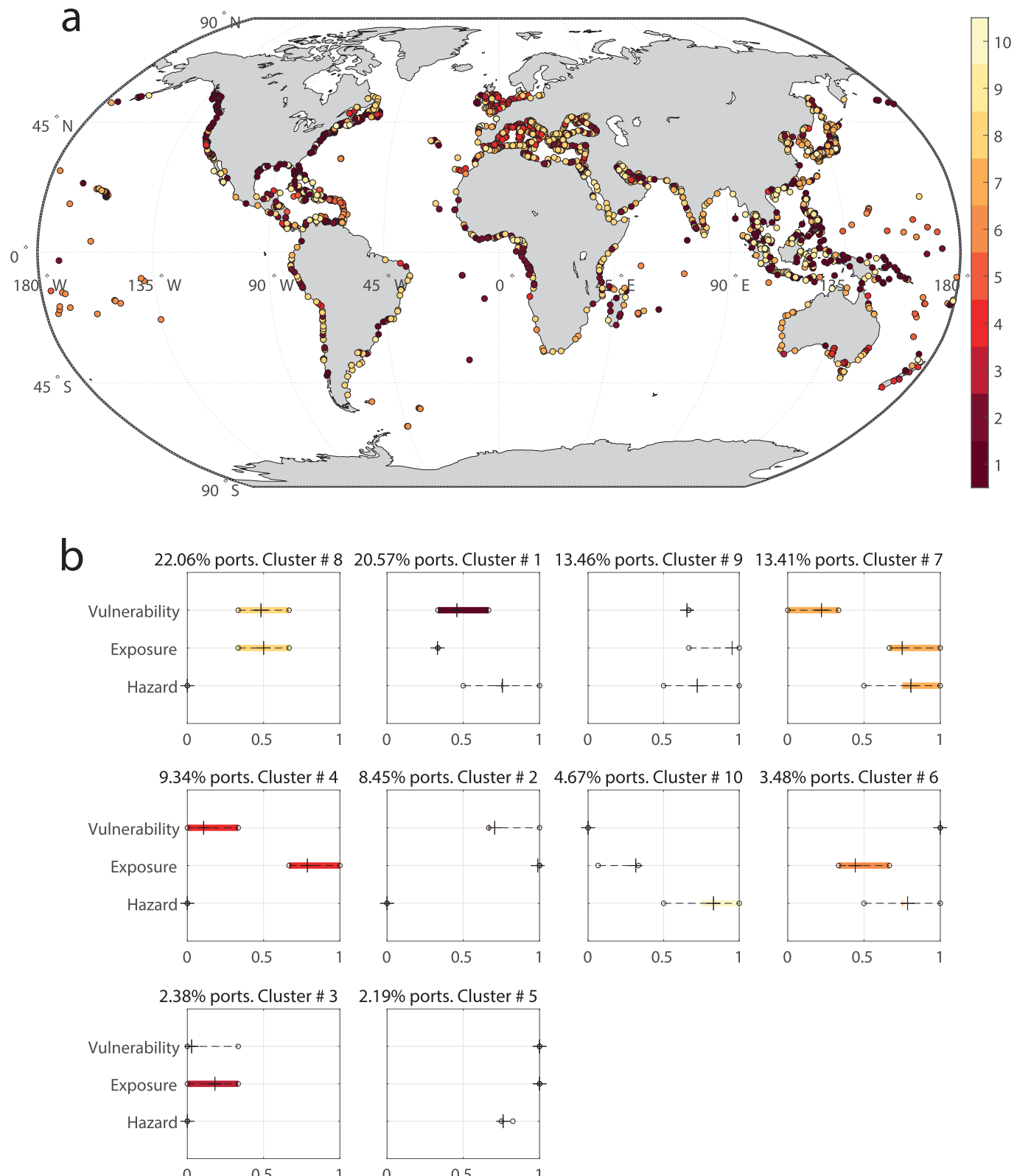


Extended Data Fig. 8 | See next page for caption.

Extended Data Fig. 8 | Multihazard change conditions in world port operations. **a**, Representative clusters of multihazard change conditions for each port in the year 2100 under RCP8.5. **b**, Characteristics of the clusters. Each panel contains the % of ports included in the cluster, the number of the cluster, the representation of the centroid (cross), the 5 and 95 percentiles of the data of the cluster (points) and the 25 and 75 percentiles of the data of the cluster (coloured line) on a normalized (0-1) scale for each frequency indicator. DaysW15 mph = average number of days per year with daily mean wind speed \geq 15 m/s; DaysT40Deg = average number of days per year with daily maximum temperature \geq 40°C; DaysP20 mm = average number of days per year with heavy precipitation (>20 mm); DaysHs2.5m = average number of days per year with significant wave height $>$ 2.5 m in the navigation zone; DaysOv0.1 l = number of days per year with overtopping flow $>$ 0.1 l/m/s; DaysCF = average number of days per year with coastal flooding; ProbTC = the annual exceedance probability of experiencing a Saffir-Simpson Hurricane Scale Category 1 or higher; and ProbMajorTC = the annual exceedance probability of experiencing a Saffir-Simpson Hurricane Scale Category 3 or higher (major hurricanes).



Extended Data Fig. 9 | Present vulnerability conditions across clusters. Present-day vulnerability conditions are shown for each port, categorized by cluster. **a**, Representative clusters of vulnerability conditions for each port. **b**, Characteristics of the clusters of vulnerability. Each panel contains the % of ports included in the cluster, the number of the cluster, the representation of the centroid (cross), the 5 and 95 percentiles of the data of the cluster (points) and the 25 and 75 percentiles of the data of the cluster (coloured line) on a normalized (0-1) scale for each vulnerability dimension: Tech. Cap = technological capacity; Resilience and Recov. Cap. = recovery capacity.



Extended Data Fig. 10 | Present risk conditions across clusters. Present-day risk conditions are shown for each port, categorized by cluster. **a**, Representative cluster of present risk conditions for each port. **b**, Characteristics of the clusters. Each panel contains the % of ports included in the cluster, the number of the cluster, the representation of the centroid (cross), the 5 and 95 percentiles of the data of the cluster (points) and the 25 and 75 percentiles of the data of the cluster (coloured line) on a normalized (0-1) scale for each frequency indicator.